

## Green synthesis of multimodal ‘OFF-ON’ switchable MRI/optical probes

J. Gallo<sup>1\*</sup>, N. Vasimalai<sup>2</sup>, M.T. Fernandez-Arguelles<sup>2</sup>, M. Bañobre-López<sup>1\*</sup>

<sup>1</sup> Advanced (magnetic) Theranostic nanostructures group, INL – International Iberian Nanotechnology Laboratory,  
Av. Mestre José Veiga, 4715-330 Braga, Portugal

<sup>2</sup> Life Sciences department, INL – International Iberian Nanotechnology Laboratory, Av. Mestre José Veiga, 4715-  
330 Braga, Portugal

### Electronic supporting information

**Table S1.** CQDs characterisation summary.

Parameters	Results
Excitation/emission maximum	$\lambda_{\text{ex}}:$ 370 nm $\lambda_{\text{em}}:$ 462 nm
Stokes shift	92 nm
FWHM	145 nm
Size (TEM)	$4.3 \pm 0.5$ nm
d-spacing (TEM)	0.32 nm
<i>D</i> band	$1340.6 \text{ cm}^{-1}$
<i>G</i> band (Raman)	$1567.5 \text{ cm}^{-1}$
$I_D/I_G$ (Raman)	1.44
Zeta potential	-16.3 mV
Quantum yield (quinine sulfate std)	38.31 %

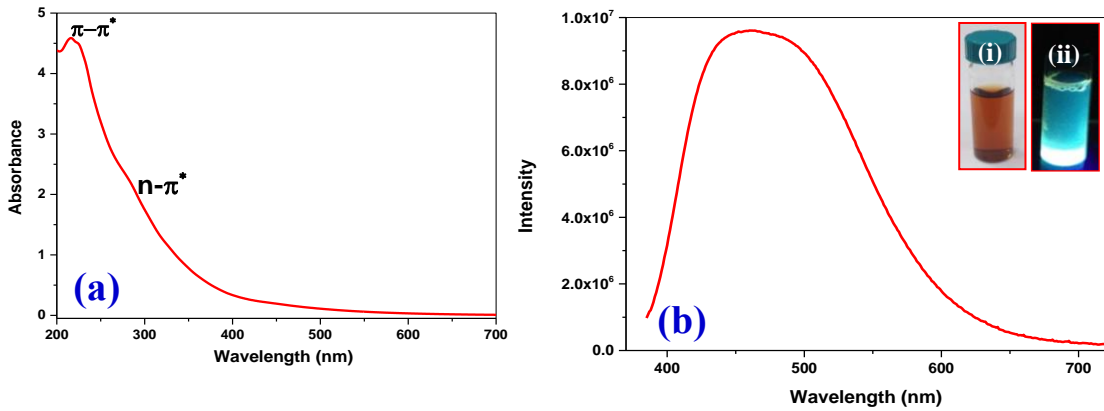


**Figure S1.** (a) UV-vis and (b) emission spectra of CQDs ( $\lambda_{\text{ex}}/\lambda_{\text{em}} = 370 \text{ nm}/462 \text{ nm}$ ). Inset: photographs of CQDs water solutions (i) day light (ii) UV light (320 nm).

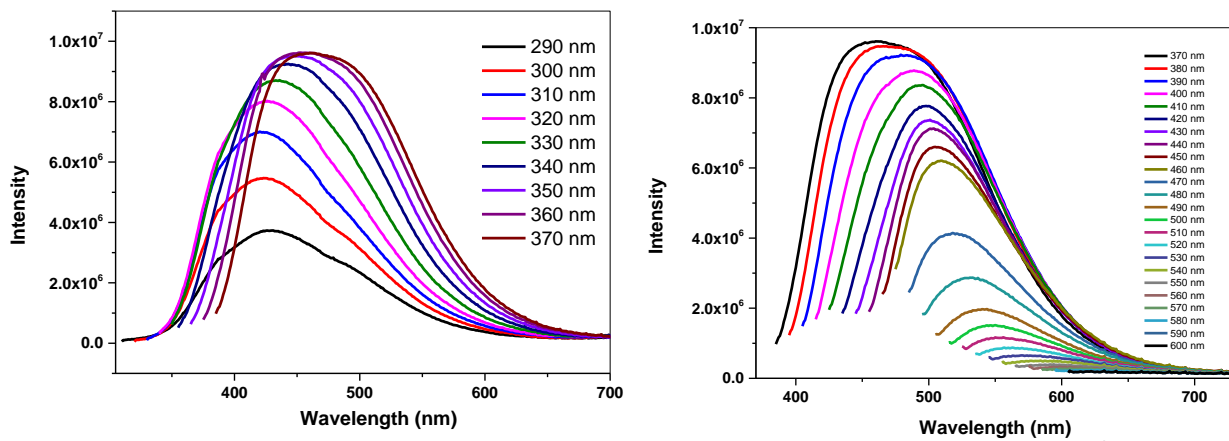


**Figure S2.** Emission spectra of CQDs under different excitation wavelengths. **Left**, from 290 to 370 nm, and **right**, from 370 to 600 nm.

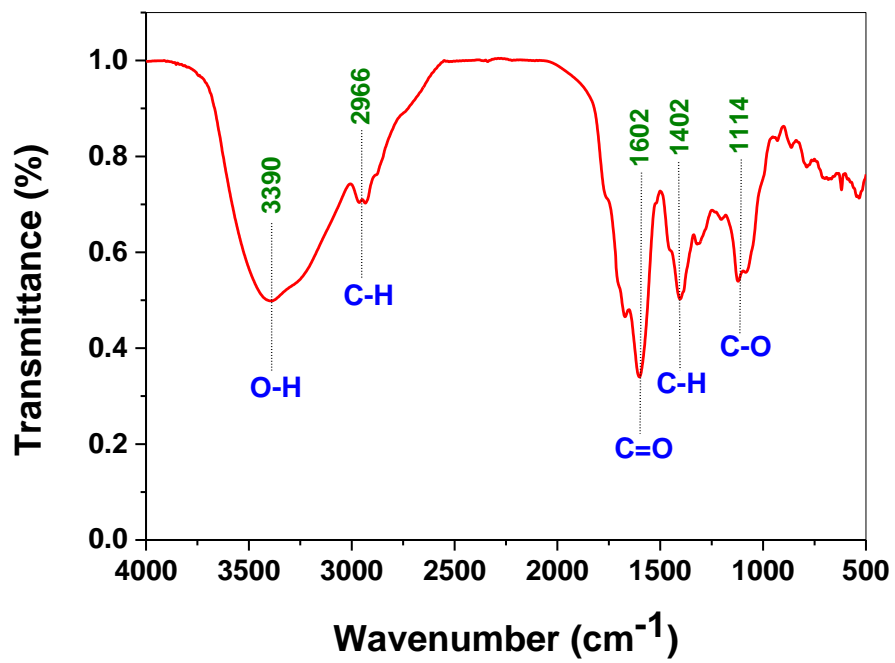


**Figure S3.** FT-IR spectrum of CQDs

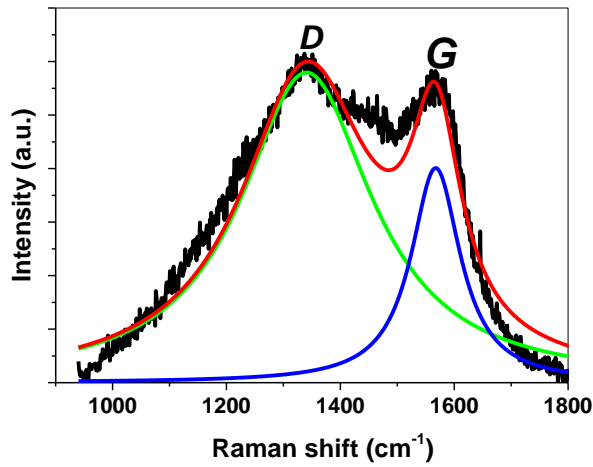


**Figure S4.** Raman spectrum of CQDs showing *D* and *G* bands.

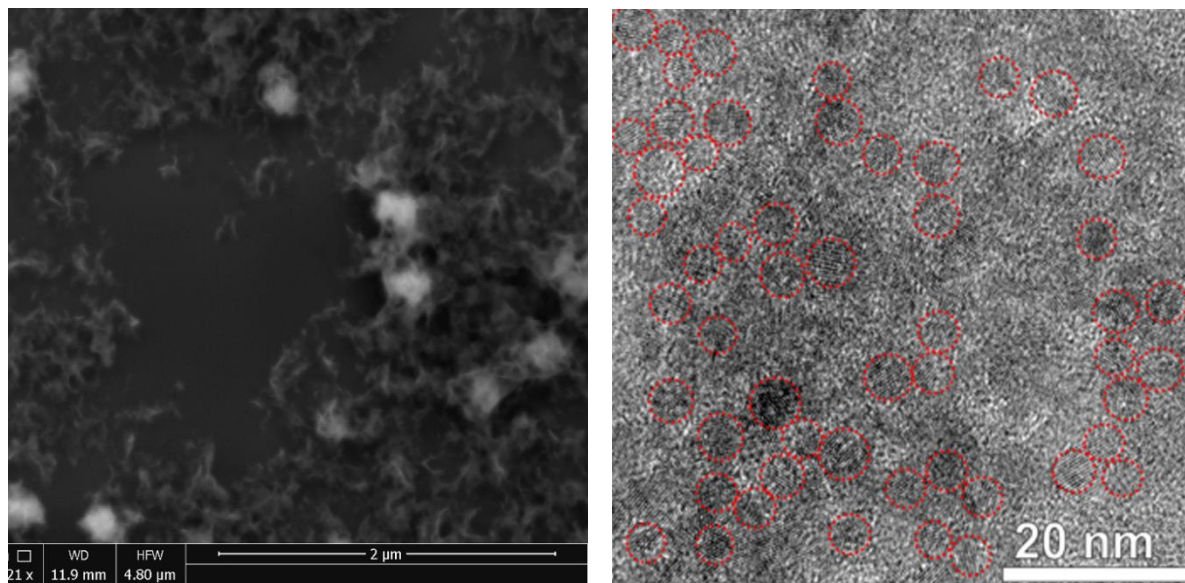


**Figure S5.** Left, overview SEM image of MnO<sub>2</sub>\_CQDS nanosheets deposited on a silicon surface. Right, high resolution TEM image of CQDs.

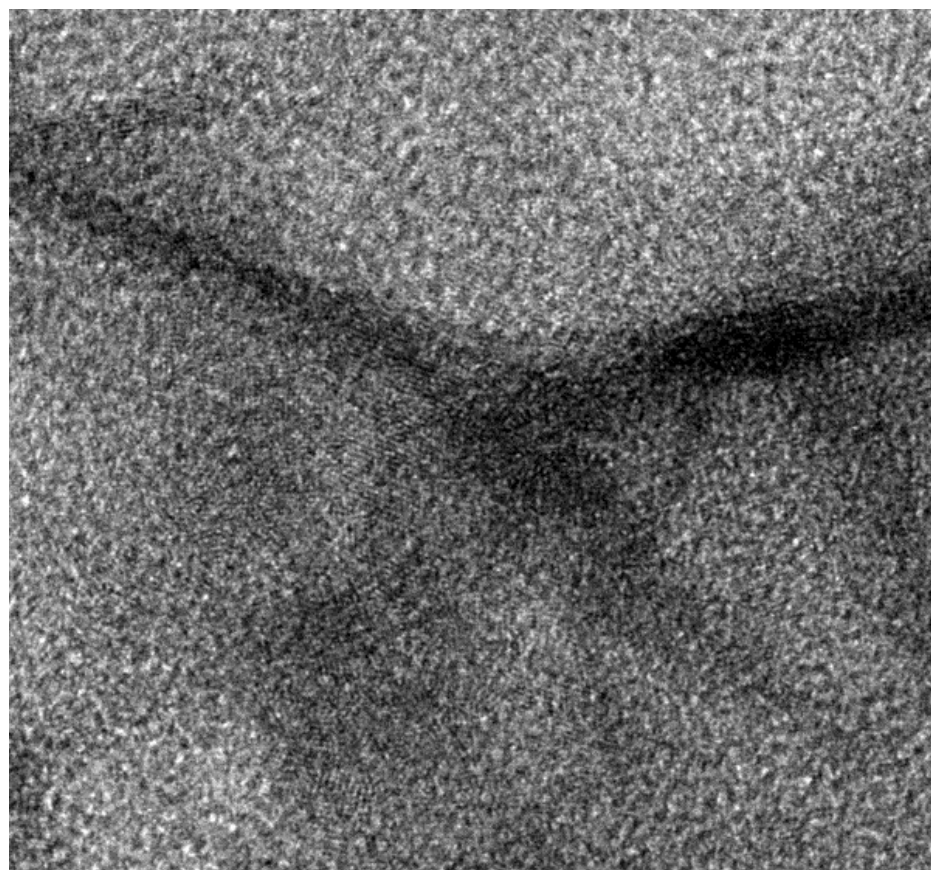
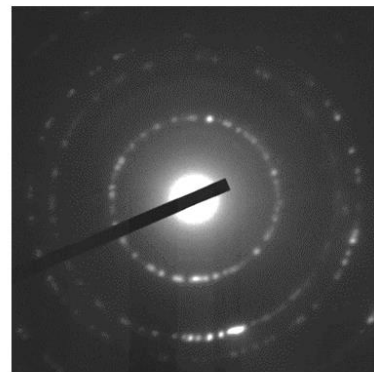


**Figure S6.** High resolution TEM image of MnO<sub>2</sub>\_CQDs showing the polycrystalline nature of the sample.



Sample	D spacing (nm)	Tentative assignment
MnO <sub>2</sub> _CQDs	0.2845{2,2,2}, 0.2596{0,0,-4}, 0.2013{2,3,3}, 0.1733{-4,4,0}, 0.1461{-1,3,-6}	MnO <sub>2</sub>

**Figure S7.** SAED pattern obtained on a sample of MnO<sub>2</sub>\_CQDs and the assignment of the structure.

### EDXS analysis

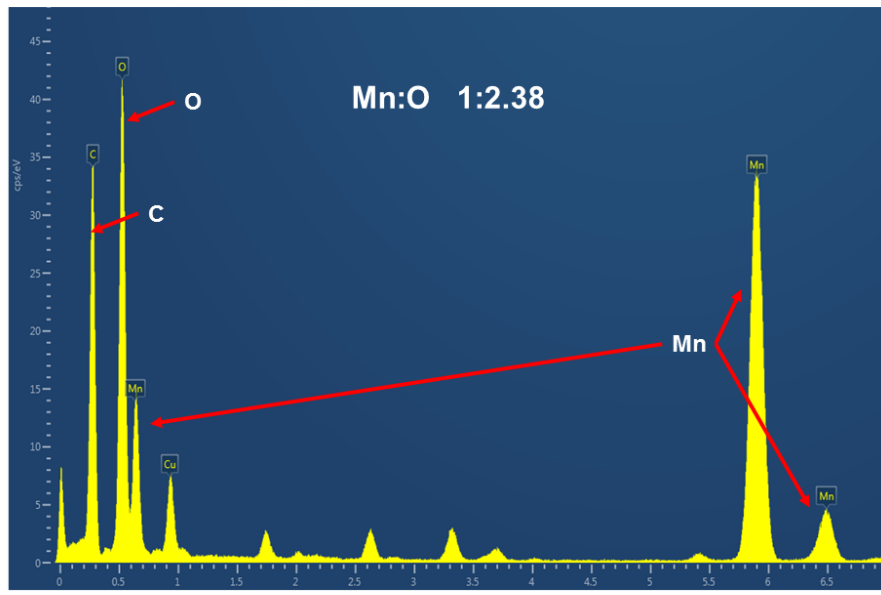
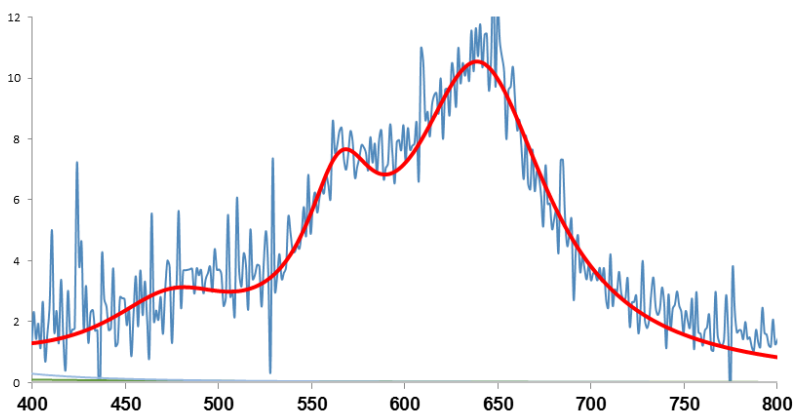


**Figure S8.** Energy dispersive X-ray spectra (EDXS) of a MnO<sub>2</sub>\_CQDs sample showing clear peaks from Mn, O and C.



Sample	Raman shift / $\text{cm}^{-1}$	Tentative assignment
MnO <sub>2</sub> _CQDs	148, 475, 565, 640	$\alpha\text{MnO}_2$ <sup>§</sup>

<sup>§</sup> *Anal.Chim.Acta*, 2009, 648(2), 235

**Figure S9.** Raman spectra and tentative assignment of the peaks of a sample of MnO<sub>2</sub>\_CQDs.

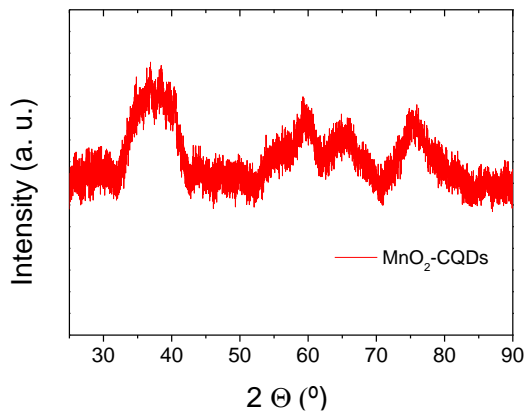


**Figure S10.** XRD diffractogram of MnO<sub>2</sub>\_CQDs nanosheets showing a pattern matching the JCPDS pattern of MnO<sub>2</sub> (JCPDS 44-0141, *J.Phys.Chem.C*, 2015, 119, 6604). The baseline signal has been subtracted by adjacent-averaging smoothing method considering 20 anchor points connected by Spline interpolation.

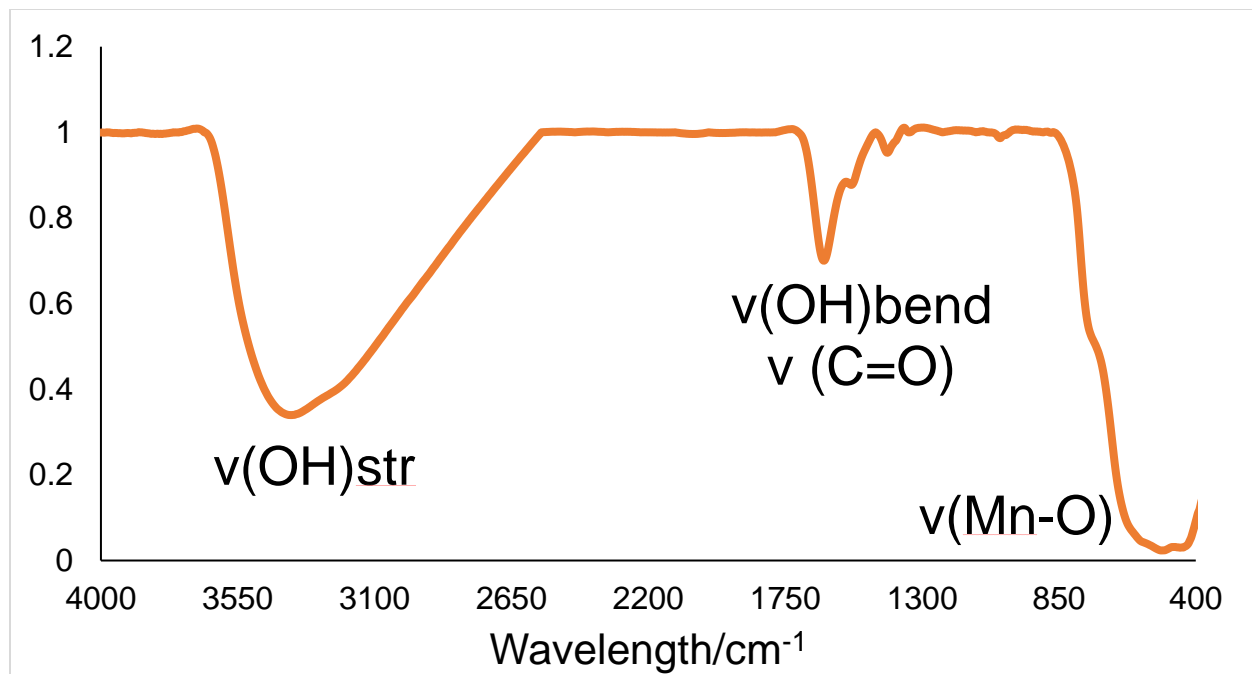


**Figure S11.** FT-IR spectra of MnO<sub>2</sub>-CQDs nanocomposites.

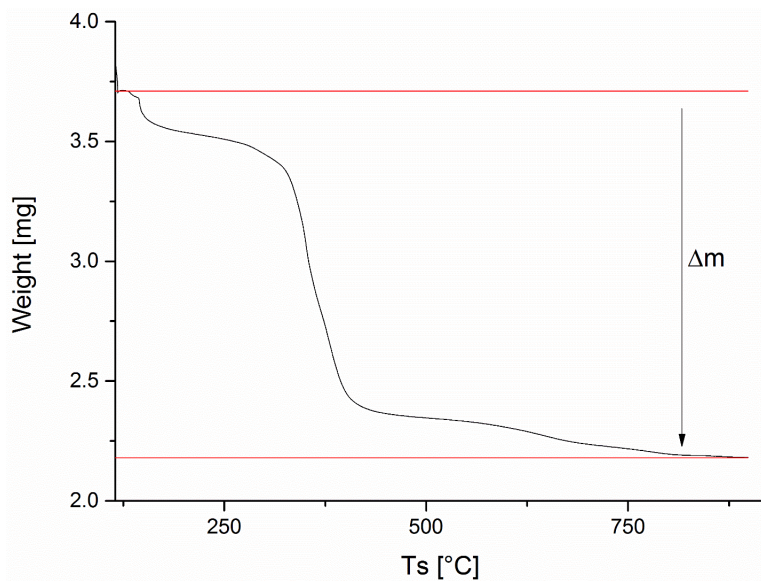


**Figure S12.** TGA curve showing the mass loss from MnO<sub>2</sub> nanosheets (after solvent loss) against temperature.

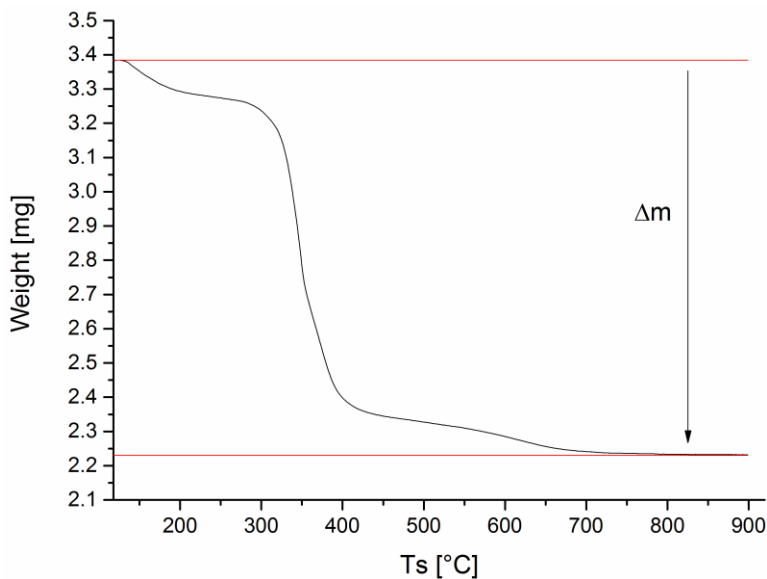


**Figure S13.** TGA curve showing the mass loss from  $\text{MnO}_2$ -CQDs nanocomposites (after solvent loss) against temperature.

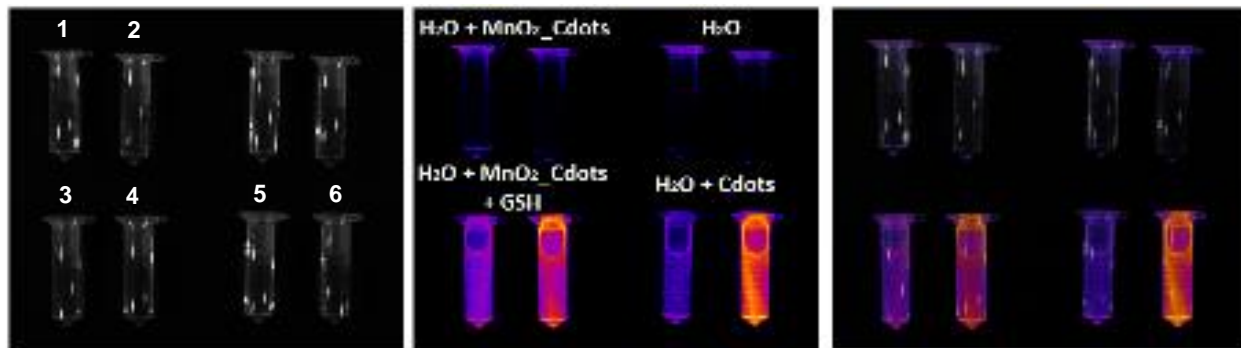


**Figure S14.** Left, white light image of water solutions of  $\text{MnO}_2$ -CQDs nanocomposites (left column) before (upper) and after (bottom) reduction with GSH, and CQDs (bottom right column); center, green channel fluorescence of the same samples; right, overlay image.  $\text{MnO}_2$ -CQDs concentration: 1 and 3, 0.9 mg Mn/mL; 2 and 4, 1.8 mg Mn/mL. CQDs concentration: 5, 0.9 mg/mL; 6, 1.8 mg/mL. GSH concentration 5 mM.

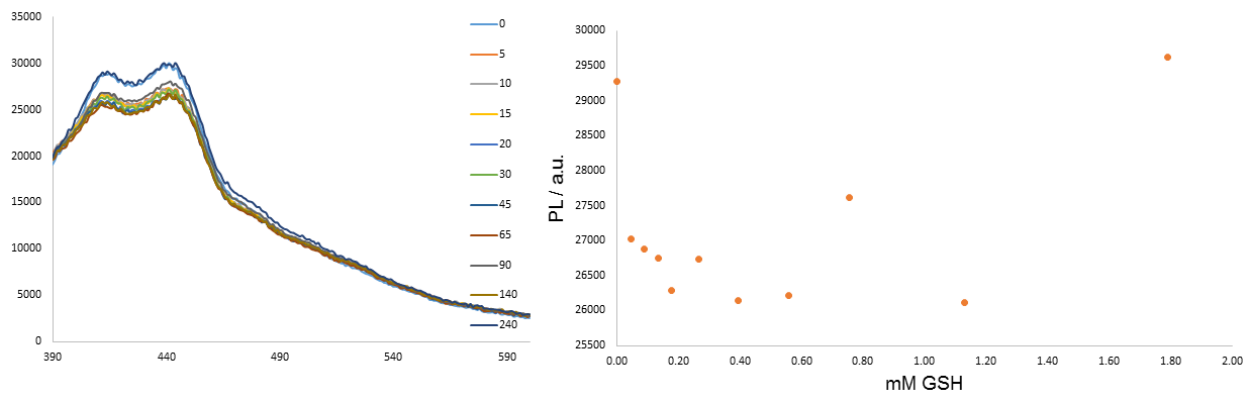


**Figure S15.** **Left**, evolution of the fluorescence spectra of a 11  $\mu\text{g Mn/mL}$  solution of  $\text{MnO}_2$ -CQDs nanocomposites in completed (10% foetal bovine serum) DMEM medium upon the addition of increasing concentrations of GSH (from 0 to 1.80 mM). **Right**, evolution of the fluorescence at 443 nm versus the concentration of GSH.

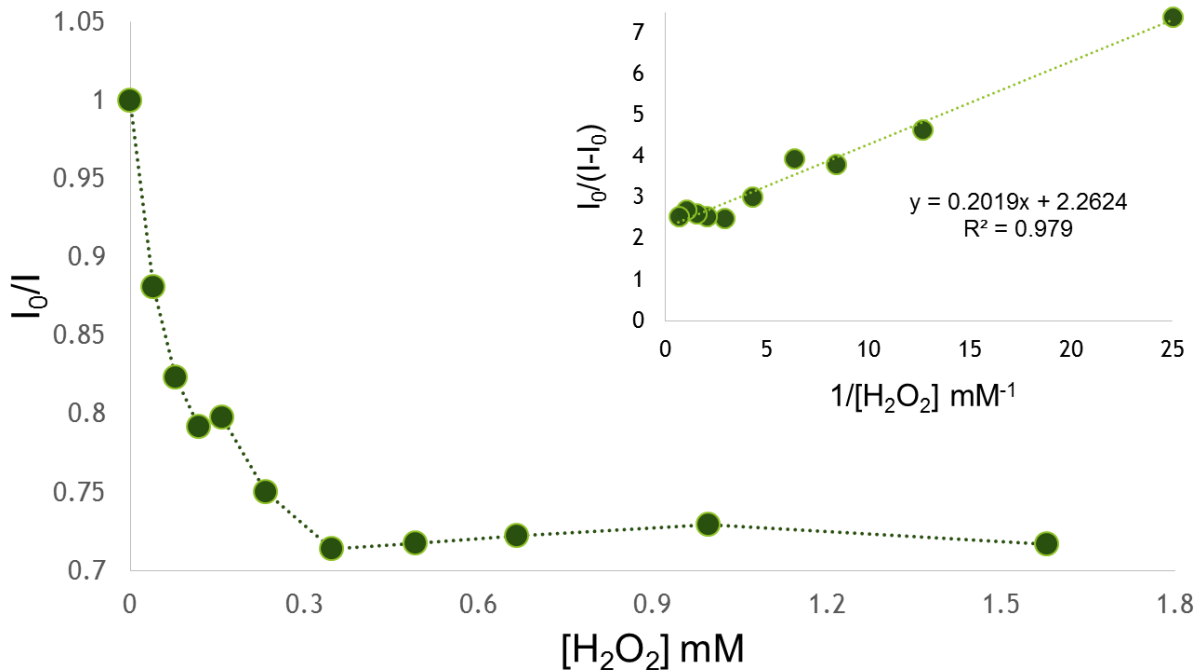


**Figure S16.** Investigation of the de-quenching mechanism of CQDs PL from  $\text{MnO}_2$  nanosheets in the presence of increasing concentrations of  $\text{H}_2\text{O}_2$ .

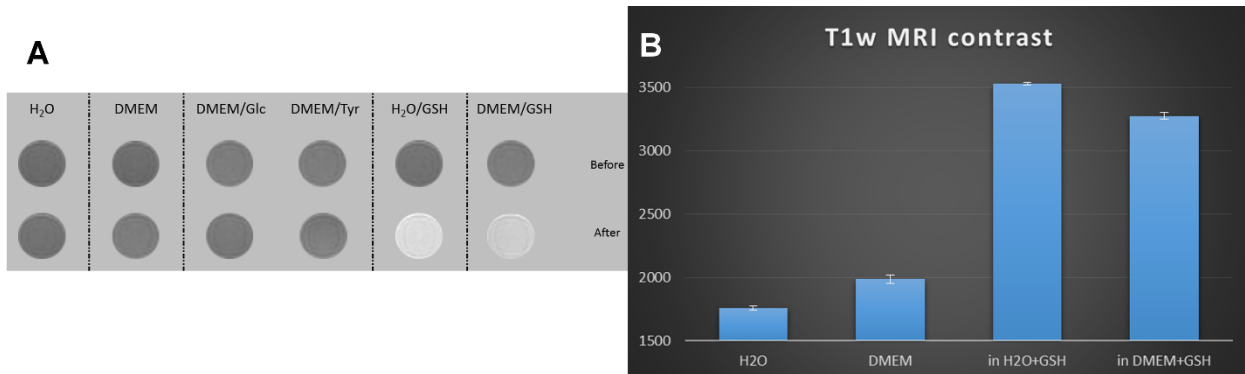


**Figure S17.** **A**,  $T_1$ -weighted MR image of different phantoms: First column,  $\text{H}_2\text{O}$  only (top) and  $\text{MnO}_2$ \_CQDs in  $\text{H}_2\text{O}$  (bottom). Second column, DMEM only (top) and  $\text{MnO}_2$ \_CQDs in DMEM (bottom). Rest of columns,  $\text{MnO}_2$ \_CQDs in DMEM or  $\text{H}_2\text{O}$  (top) and  $\text{MnO}_2$ \_CQDs in DMEM or  $\text{H}_2\text{O}$  after the addition of Glc, Tyr, or GSH (bottom). **B**, Signal intensity analysis from phantoms in A showing a clear OFF-ON transition both in water and DMEM cell culture media.

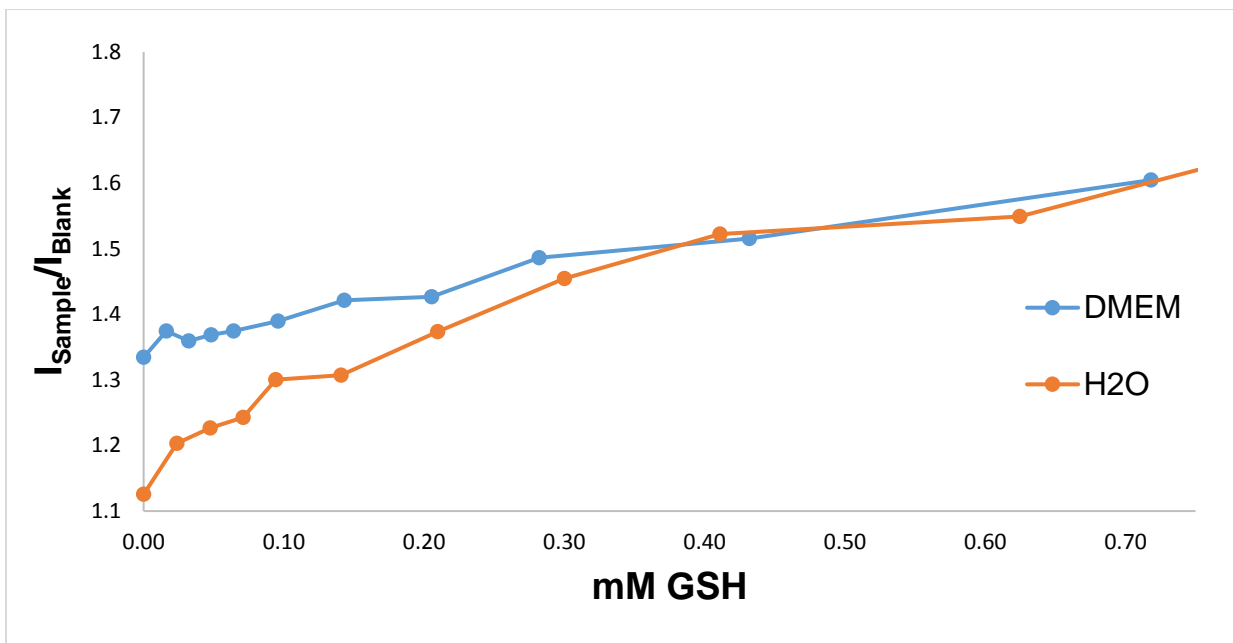


**Figure S18.** Evolution of the  $T_1$ -weighted signal intensity of a phantom containing 6 ug Mn/mL of MnO<sub>2</sub>-CQDs in water (orange) or completed DMEM cell culture media (blue) as a function of the concentration of GSH in the solution.

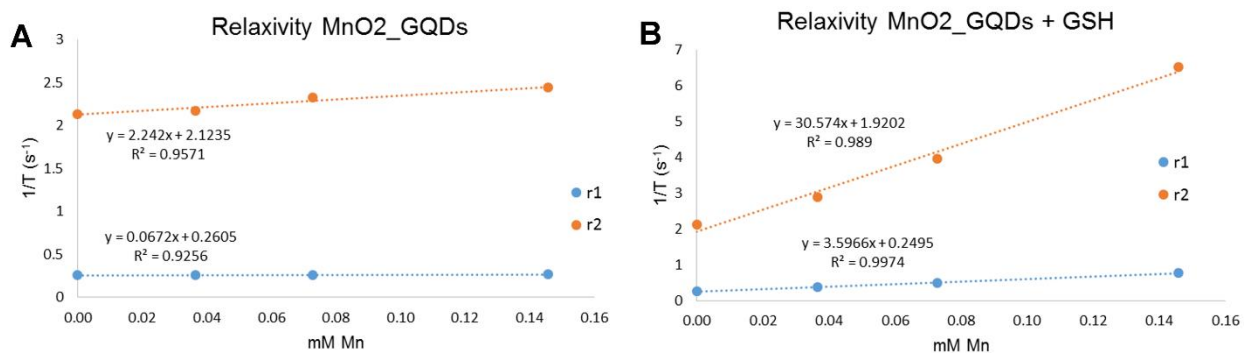


**Figure S19.**  $r_1$  and  $r_2$  relaxivity plots of MnO<sub>2</sub>-CQDs nanocomposites in water before (A) and 24h after (B) the addition of 100 mM GSH.

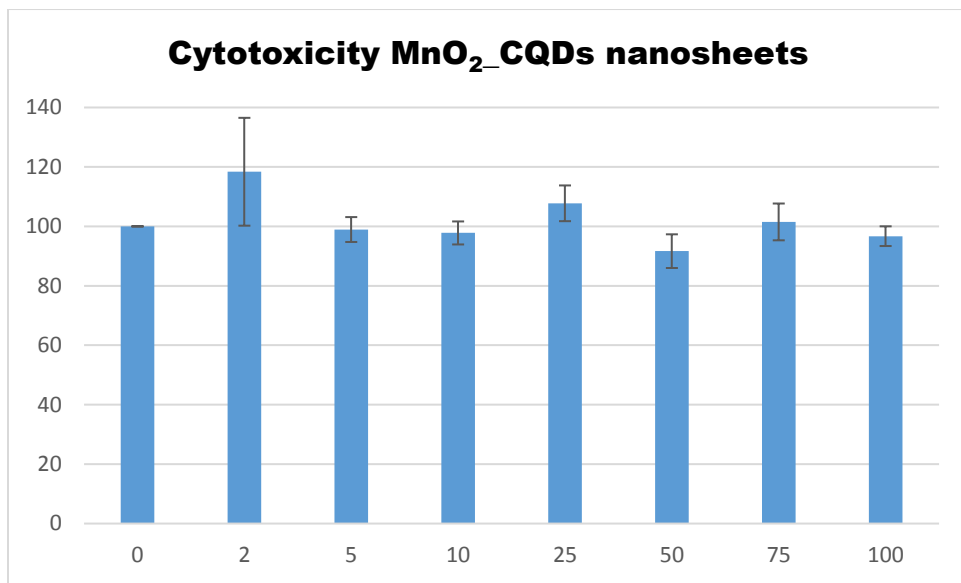


**Figure S20.** Viability test of A549 cells incubated for 4h at 37°C and 5% CO<sub>2</sub> in the presence of increasing concentrations of MnO<sub>2</sub>-CQDs (0 to 100  $\mu\text{g Mn/mL}$ ).

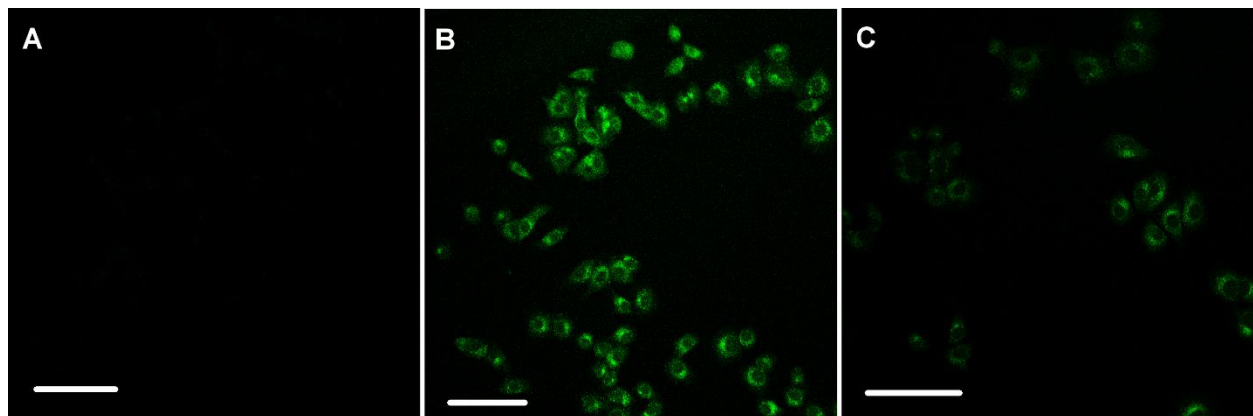


**Figure S21.** Representative fluorescence confocal images of A549 cells incubated only in completed DMEM cell culture media (**A**), completed cell culture media plus 1.8 mg/mL of turmeric CQDs (**B**), and completed cell culture media plus 1.8 mg Mn/mL of MnO<sub>2</sub>-CQDs nanocomposites (**C**).